Linking circadian time to growth rate quantitatively *via* carbon metabolism

Yin Hoon Chew[1†], Daniel D. Seaton[1], Virginie Mengin[2], Anna Flis[2], Sam T. Mugford[3], Alison M. Smith[3], Mark Stitt[2], Andrew J. Millar*[1]

Affiliations:

[1] SynthSys and School of Biological Sciences, C. H. Waddington Building, University of Edinburgh, King's Buildings, Edinburgh EH9 3BF, United Kingdom

[2] Max Planck Institute of Molecular Plant Physiology, Am Muehlenberg 1, 14476 Potsdam-Golm, Germany

[3] Department of Metabolic Biology, John Innes Centre, Norwich NR4 7UH, United Kingdom

*Corresponding author : Andrew J. Millar

Complete address : SynthSys

C.H. Waddington Building

University of Edinburgh

Max Born Crescent

Edinburgh EH9 3BF

Scotland, UK

Telephone number : +44 (0)131 651 3325

Email : Andrew.Millar@ed.ac.uk

[†]**Current address (YHC)** : Department of Genetics & Genomic Sciences, Icahn Institute for Genomics & Multiscale Biology, Icahn School of Medicine at Mount Sinai, 1425 Madison Avenue, New York, NY 10029-6574, USA

Keywords: gene regulatory dynamics; metabolism; genotype to phenotype; mathematical model

Summary paragraph (200 words)

Predicting a multicellular organism's phenotype quantitatively from its genotype is challenging, as genetic effects must propagate up time and length scales. Circadian clocks are intracellular regulators that control temporal gene expression patterns and hence metabolism, physiology and behaviour, from sleep/wake cycles in mammals to flowering in plants[1-3]. Clock genes are rarely essential but appropriate alleles can confer a competitive advantage[4,5] and have been repeatedly selected during crop domestication[3,6]. Here we quantitatively explain and predict canonical phenotypes of circadian timing in a multicellular, model organism. We used metabolic and physiological data to combine and extend mathematical models of rhythmic gene expression, photoperiod-dependent flowering, elongation growth and starch metabolism within a Framework Model for growth of *Arabidopsis thaliana*[7-9]. The model predicted the effect of altered circadian timing upon each particular phenotype in clock-mutant plants. Altered night-time metabolism of stored starch accounted for most but not all of the decrease in whole-plant growth rate. Altered mobilisation of a secondary store of organic acids explained the remaining defect. Our results link genotype through specific processes to higher-level phenotypes, formalising our understanding of a subtle, pleiotropic syndrome at the whole-organism level, and validating the systems approach to understand complex traits starting from intracellular circuits.

51 (Text 1507 words)

52 Small networks of "clock genes" drive 24-hour, biological rhythms in eukaryotic model
53 species[1]. A few among thousands of downstream, clock-regulated genes are known to mediate
54 physiological phenotypes, such as the metabolic syndrome of clock mutant animals[10].
55 Identifying such causal links cannot predict whole-organism phenotypes quantitatively: formal,
56 mathematical models are required. Predictive modelling in multicellular organisms has best
57 succeeded for phenotypes that closely map the intracellular behaviour of gene circuits[11],
58 metabolic[12] or signalling pathways[13]. Circadian clocks in contrast integrate multiple
59 environmental inputs and affect disparate, potentially interacting biological processes, up to
60 organismal growth and lifecycle traits[4,14]. Mis-timed mutant organisms suffer a syndrome of
61 mild, environment-dependent effects akin to a chronic disease[1,4,10].

62 The Arabidopsis clock mechanism[1] comprises dawn-expressed transcription factors *LATE*
63 *ELONGATED HYPOCOTYL* (*LHY*) and *CIRCADIAN CLOCK-ASSOCIATED 1* (*CCA1*),
64 which inhibit the expression of evening genes such as *GIGANTEA* (*GI*) (Fig.1a). *LHY* and
65 *CCA1* expression is inhibited by PSEUDO-RESPONSE REGULATOR (PRR) proteins.
66 Removing the earliest-expressed *PRR* genes in *prr7prr9* mutants slows the clock[15] by delaying
67 the decline of *LHY* and *CCA1* expression and the subsequent rise of their targets (Fig.1b).
68 Mathematical models of this circuit[16] have been extended to intermediate transcription factors,
69 including factors that regulate flowering time and organ elongation[7]. We therefore tested
70 whether these causal links were sufficient to understand (explain and predict) the multiple
71 phenotypes of a clock mutant genotype.

72 The Arabidopsis Framework Model (FMv1)[9] represents the interacting physiological
73 components of whole-organism phenotypes, in a simple, modular fashion. Flowering time in
74 Arabidopsis is commonly scored by the number of rosette leaves, for example. Predicting leaf
75 number involves the FM's clock and photoperiod[7], phenology[17] and functional-structural sub-

76 models[18]. Adding a clock sub-model that explicitly represents *PRR7*, *PRR9* and output
77 pathways (see Supplementary Methods; Fig.2) was sufficient to match the published, late-
78 flowering phenotype[19] of *prr7prr9* compared to wild-type Columbia (Col) plants under long
79 photoperiods (Fig.1c). Under short photoperiods, the mutant phenotype is weaker (Extended
80 Data Fig.1a). The model also matched the observed[20], photoperiodic regulation of hypocotyl
81 elongation in wild-type plants and qualitatively matched the longer hypocotyls of *prr7prr9*
82 (Extended Data Fig.1b).

83 Biomass growth is mediated by the metabolic network, the development of sink and source
84 organs and resource partitioning amongst them. Here, we test the importance of one of many
85 potential circadian effects on biomass, *via* the nightly, clock-limited rate of sugar mobilisation
86 from storage in transient starch[21]. To understand these carbon dynamics in *prr7prr9*, we first
87 extended the metabolic sub-model. Daytime starch accumulation in wild-type plants under
88 short photoperiods was underestimated in the FMv1[9,22]. Partitioning of photoassimilate
89 towards starch in the model was therefore updated using the measured activity of the key
90 biosynthetic enzyme, AGPase, which partitions more carbon to starch under short photoperiods
91 than is allowed for in the FMv1 (Supplementary Methods; Extended Data Fig.2a). At night,
92 starch is mobilised (degraded) at a constant rate to provide sugar until dawn, as anticipated by
93 the circadian clock[21,23]. We therefore linked the starch degradation rate to the clock sub-model[8]
94 (Supplementary Methods). Simulation of the revised model closely matched end-of-day starch
95 levels under photoperiods of 12h or less (Fig.1e). Finally, the organic acids malate and fumarate
96 also accumulate significantly during the day in Arabidopsis, are mobilised at night and have
97 been proposed as secondary carbon stores[24]. At the end of the day, levels of malate and
98 fumarate were two-fold higher in *prr7prr9* than wild-type, with a smaller elevation of citrate,
99 aconitate and iso-citrate (Figs.1d, Extended Data Fig.3). Malate and fumarate were therefore
100 included as an organic acid pool with dynamics similar to starch, in an extended model termed

101 the FMv2 (Fig.2). The FMv2 predicts the gain of carbon biomass directly and other major
102 biomass components indirectly. For example, the 3.3-fold increase in protein synthesis rates
103 from night to day predicted by the model was very close to the observed 3.1-fold increase[25](see
104 Supplementary Methods). If altered starch mobilisation in the clock mutant was sufficient to
105 affect its biomass, the FMv2 should also predict that phenotype.

106 We first tested whether the FMv2 could explain the phenotypes caused by a direct change in
107 starch degradation, in mutants of *LIKE SEX FOUR 1* (*LSF1*). *LSF1* encodes a phosphatase
108 homologue necessary for normal starch mobilisation[26]. *lsf1* mutants grown under 12L:12D
109 have mildly elevated starch levels and reduced biomass[26], similar to the *prr7prr9* clock mutant
110 (Fig.3b). Reducing the relative starch degradation rate alone in the FMv2 recapitulated the *lsf1*
111 starch excess observed in published studies[26] (Extended Data Fig.1c) and new datasets
112 (Figs.3g,3i). The higher baseline starch level arises naturally if the plant is close to a steady
113 state, where the absolute amount of starch degraded nightly in *lsf1* equals the daily synthesis.
114 Absolute starch synthesis in *lsf1* is wild-type (Fig.3g,3i). To degrade the same amount of starch
115 as wild-type at a lower relative rate, the *lsf1* mutant must have a higher baseline starch level.
116 The assumption of a lower relative degradation rate in *lsf1* is therefore functionally equivalent
117 to but conceptually simpler than the previous assumption of an altered 'starch set point'
118 baseline level[23,26].

119 A minimal model calibration workflow (Extended Data Fig.4) allowed comparison of
120 simulations of the FMv2 with measurements from multiple experiments on *prr7prr9* and *lsf1*
121 mutants. Measured photosynthetic and metabolic variables (Extended Data Fig.5) calibrated
122 up to 4 model parameters (Extended Data Table 1), and the genotype-specific water content[9].
123 Reducing the relative starch degradation rate in the calibrated model accurately predicted the
124 reduced biomass of *lsf1* mutant plants in each case (Figs.3c,3e), despite the apparent paradox
125 that the mutants mobilised the same absolute amount of starch as the wild type. The explanation

126 supported by the model is that *lsf1* mutant plants accumulate large, unused starch pools as well
127 as new biomass, whereas wild-type plants produce biomass more efficiently, leaving only a
128 minimum of carbon in starch. The coefficient of variation of the Root-Mean-Square Error
129 (cvRMSE) provides a normalised error metric for all biomass data[9], showing a good fit to both
130 *lsf1* and wild-type genotypes (10.1%, 15.3% Col and 13.7%, 15.4% *lsf1* in experiments 1 and
131 2 respectively). Altering the relative starch degradation rate therefore explained both the *lsf1*
132 mutant's modest starch excess and its reduced biomass, validating the model.

133 *prr7prr9* mutants showed slower relative starch degradation (Fig.3a) and higher starch levels
134 at both dawn and dusk (Extended Data Fig.1d) than the wild type. Simulating *prr7prr9*
135 mutations in the clock sub-model matched these phenotypes for plants grown in Norwich
136 (Figs.3a, Extended Data 1e) and Edinburgh (Fig.3h), indicating that the mutant clock's later
137 estimate of subjective dawn explained the starch degradation defect. *prr7* single mutants[27] fully
138 mobilised starch and grew normally, as predicted (Extended Data Fig.6). Although model
139 calibration data showed that photosynthesis, starch synthesis and leaf production rates were
140 unaffected by the mutations (Extended Data Fig.5), biomass of *prr7prr9* mutant plants was
141 strongly reduced relative to wild-type plants in independent studies (by 40% and 31% at 38
142 days in experiments 1 and 2 respectively). However, the calibrated FMv2 predicted much
143 smaller reductions in biomass in *prr7prr9* due to accumulating starch (26% and 18% in
144 experiments 1 and 2 respectively). Neither 1 S.D. variation in the mutant's simulated water
145 content, the most sensitive parameter in our model (Extended Data Fig.7), nor any measured
146 water content value allowed the model with only a starch defect to match the mutant biomass
147 (Extended Data Fig.8). The poor model fits (cvRMSE = 41%, 45% in experiments 1 and 2
148 respectively) indicated that process(es) additional to starch degradation limited the growth of
149 *prr7prr9* but not of *lsf1* plants.

150 Considering malate and fumarate as a secondary carbon store[24], the amount of carbon
151 mobilised from malate and fumarate at night in the wild type was up to 19% of the carbon
152 mobilised from starch. *prr7prr9* but not *lsf1* plants accumulated excess malate and fumarate,
153 representing further 'wasted' carbon that did not contribute to subsequent growth (Figs.3k-n).
154 We therefore reduced the relative malate and fumarate mobilisation rate in the FMv2
155 simulation of *prr7prr9,* to reproduce the observed organic acid excess (Figs.3l,3n). Together,
156 the simulated defects in starch and organic acid mobilisation quantitatively accounted for the
157 mutant's reduced biomass (Figs.3d,3f; cvRMSE = 14.4%, 20.1% in experiments 1 and 2
158 respectively).

159 The FMv2 built upon delayed gene expression patterns in *prr7prr9* mutants to predict canonical
160 clock phenotypes: altered hypocotyl elongation, flowering time, starch metabolism and hence
161 most (58-65%) of the mutants' reduced biomass. Unused malate and fumarate accounted for
162 their remaining biomass defect, and might similarly affect arrhythmic *prr5prr7prr9* mutants[28].
163 Carbon supply limited growth in our well-watered, nutrient-rich growth conditions[22], though
164 carbon limitation was milder than in conditions that reduced the chlorophyll content of clock
165 mutants[4] or triggered sugar signals to alter timing[27]. Future extensions of the model could
166 address the nutrient and water limitations that prevail in field conditions, test further aspects of
167 circadian regulation and critical functions of plant biology with daily regulation, such as
168 photosynthesis. Our results suggest a broader proof of principle, that the contributions of
169 dynamic gene regulation and metabolism to whole-organism physiology will also be
170 understood (explained and predicted) quantitatively in other multicellular species[29], for
171 example using clock and metabolic models in animals and humans to understand body
172 composition[10].

173

Acknowledgements

Supported by European Commission FP7 collaborative project TiMet (contract 245143) and by a BBSRC Institute Strategic Programme Grant BB/J004561/1 to the John Innes Centre.

Author Contributions

YHC, AS, MS and AJM designed the study. YHC, VM, AF, SM, AS and MS performed the experiments and analysed the experimental data. YHC and DDS performed the modelling and analysed the simulation results. YHC, DDS and AJM wrote the paper with input from all authors.

Figure legends

Figure 1: Simulation of clock dynamics and clock outputs.

(a,b) Clock gene mRNA abundance[30] for wild-type (Col) and *prr7prr9* plants (dashed lines, symbols), and FMv2 simulations (solid lines), under 12h light:12h dark cycles (12L:12D), double-plotted, normalised to Col level. (c) Rosette leaf number at flowering[19] under 16L:8D (filled), compared to simulation (open). (d) Malate and fumarate accumulation (mean±SEM, n=4) in Col and *prr7prr9* at end of day (ED) or night (EN) under 12L:12D, 20°C, light intensity=160 μmol/m^2/s; t-tests compared *prr7prr9* to Col (* $p<0.05$; *** $p<0.001$). (e) Starch levels at ED (filled) and EN (open) after 30 days under various photoperiods[22] (triangles), compared to FMv1 (squares), FMv2 (circles).

196 Figure 2: Schema of the Framework Model.

197 The FMv2 includes a clock gene circuit sub-model (upper section). Clock outputs (red arrows)
198 regulate hypocotyl elongation *via* the *PIF* components, flowering *via FT* mRNA production
199 and starch degradation *via* the timer *T*. Environmental inputs affect multiple model components
200 (shaded). Vegetative growth is driven by the positive feedback on photosynthesis, mediated by
201 sugar-powered growth of photosynthetically active leaf area within the plant structure. The
202 FMv2 includes nightly carbon storage both in starch and in a secondary, organic acid pool,
203 comprising malate and fumarate (Mal+Fum). Components tested by mutation (PRR9, PRR7,
204 LSF1) are shown in red (see Extended Data).

205

206 Figure 3: Contributions of starch and organic acids to biomass growth.

207 (a) *prr7prr9* (blue, squares) mobilised starch more slowly than Col (green, circles); normalised
208 to Col peak (mean±SEM, n=6). (b) 38-day-old Col, *lsf1*, *prr7prr9*. (c-n) Data (symbols) and
209 simulation (lines) of fresh weight (c-f), starch (g-j) and total malate and fumarate (k-n) for Col
210 (circles, green), *lsf1* (triangles, orange) and *prr7prr9* (squares; dashed black, simulation of
211 starch defect; blue, starch and organic acid defects). (d,f) Insets enlarge main panel. Data show
212 mean±SD; n=5 for biomass; n=3 for metabolites, where each sample pooled 3 plants.
213 Temperature=20°C (a), 20.5°C (b, Experiment1), 18.5°C (Experiment2); 12L:12D light
214 intensity=190 μmol/m^2/s (a), 145 μmol/m^2/s (b-n); CO_2=420 ppm.

Methods

Experimental methods

Plant materials and growth conditions

Arabidopsis thaliana of the Columbia (Col-0) accession, *prr7-3/prr9-1*[19] and *lsf1-1*[26] were used in this study. Seeds were first sown on half strength Murashige and Skoog (MS) solution and stratified in darkness at 4°C for 5 days before being exposed to white light at the desired photoperiod and temperature. Four-day-old seedlings were then transferred to soil containing Levington seed and modular compost (plus sand). The growth and treatment conditions for each experiment are shown in the figure legends. For the experiment in Fig.1d and Extended Data Fig.3 only, seeds were sown on wet soil in pots and transferred directly to experimental conditions. Plants were thinned after a week and treated with Nematodes after two weeks as a biological pest control.

Leaf number and plant assay

The total number of leaves (including the cotyledons) was recorded every 3-4 days from seedling emergence. Only leaves exceeding 1 mm^2 in size (by eye) were considered in the total leaf count. Plants were harvested for biomass at different time points and for metabolite measurement at 3 weeks (Extended Data Fig.3) and 4 weeks (other data). For metabolite measurement, rosettes were harvested and immediately submerged in liquid nitrogen, half an hour before lights off (end of day, ED) or lights on (end of night, EN) and stored at -80°C until extraction. For dry biomass, dissected plants were oven-dried at 80°C for 7 days. Area analysis was conducted using ImageJ [31]. Each image was first processed with colour thresholding to isolate the green region, which was next converted into binary format. The area was then determined using the Analyze Particles tool.

Gas exchange measurement

An EGM-4 Environmental Gas Monitor for CO_2 (PP Systems, US) was used for CO_2 flux measurement. A Plexiglass cylindrical chamber (12 cm in diameter x 3 cm sealed height, with a 6 cm tall support) was used (Extended Data Fig.5f). Rubber rings around the lid and the hole for the pot ensured an airtight seal. The chamber was connected to the EGM-4 with two butyl tubes for closed-loop measurement.

Each individual measurement was taken by placing an individual plant pot in the chamber for approximately 60 seconds, during which the EGM-4 recorded CO_2 concentration (μmol mol^{-1} or ppm) every 4.6 seconds. We covered the soil surface of the pots with black opaque plastic, leaving only a small hole in the middle for the plants. Plants were measured when they were 37 days old. Dark respiration was measured one hour before lights-on while daytime assimilation was measured one hour before lights-off.

CO_2 enrichment of the atmosphere in the growth chambers due to the experimenters' breathing was avoided by using a breath-scrubbing device during measurement. Hourly CO_2 concentration at leaf level was also monitored by connecting the EGM-4 to a computer for automated data logging. The average hourly CO_2 level was used as input to the model.

Extraction and determination of metabolite content

Rosettes were harvested as described above and ground in liquid nitrogen. Around 20mg of ground material was aliquoted in screw-cap tubes (Micronic). Ethanolic extraction was performed using 80% ethanol v/v with 10mM MES (pH 5.9) and 50% ethanol v/v with 10mM MES (pH 5.9). During extraction, the successive supernatants obtained were combined into 96-deep well plates. The supernatant was used for spectrophotometric determination of chlorophylls, soluble carbohydrates, amino acids and organic acids as described[32]. The pellet

remaining after the ethanolic extraction was used for the determination of starch and total protein content as described[33].

Modelling methods

Development of the FMv2 in Matlab (Mathworks, Cambridge, UK), model equations, experimental data for model calibration and simulation procedures are described in the Supplementary Methods section.

Data and model availability

A simulator to run the FMv2 in multiple conditions is publicly accessible online at http://turnip.bio.ed.ac.uk/fm/. Numerical data and model files will be available from the University of Edinburgh DataShare www.datashare.ed.ac.uk [insert doi].

References

1 Millar, A. J. The intracellular dynamics of circadian clocks reach for the light of ecology and evolution *Annu Rev Plant Biol* **67**, 595-618, doi:10.1146/annurev-arplant-043014-115619 (2016).

2 Bass, J. & Takahashi, J. S. Circadian integration of metabolism and energetics. *Science* **330**, 1349-1354 (2010).

3 Bendix, C., Marshall, C. M. & Harmon, F. G. Circadian Clock Genes Universally Control Key Agricultural Traits. *Mol Plant* **8**, 1135-1152, doi:10.1016/j.molp.2015.03.003 (2015).

4 Dodd, A. N. *et al.* Plant circadian clocks increase photosynthesis, growth, survival, and competitive advantage. *Science* **309**, 630-633, doi:10.1126/science.1115581 (2005).

5 Ouyang, Y., Andersson, C. R., Kondo, T., Golden, S. S. & Johnson, C. H. Resonating circadian clocks enhance fitness in cyanobacteria. *Proc Natl Acad Sci U S A* **95**, 8660-8664 (1998).

6 Muller, N. A. *et al.* Domestication selected for deceleration of the circadian clock in cultivated tomato. *Nat Genet*, doi:10.1038/ng.3447 (2015).

7 Seaton, D. D. *et al.* Linked circadian outputs control elongation growth and flowering in response to photoperiod and temperature. *Mol Syst Biol* **11**, 776, doi:10.15252/msb.20145766 (2015).

8 Seaton, D. D., Ebenhoh, O., Millar, A. J. & Pokhilko, A. Regulatory principles and experimental approaches to the circadian control of starch turnover. *J R Soc Interface* **11**, 20130979, doi:10.1098/rsif.2013.0979 (2014).

9 Chew, Y. H. *et al.* Multiscale digital Arabidopsis predicts individual organ and whole-organism growth. *Proc Natl Acad Sci U S A* **111**, E4127-4136, doi:10.1073/pnas.1410238111 (2014).

10 Peek, C. B. *et al.* Circadian clock NAD+ cycle drives mitochondrial oxidative metabolism in mice. *Science* **342**, 1243417, doi:10.1126/science.1243417 (2013).

11 von Dassow, G., Meir, E., Munro, E. M. & Odell, G. M. The segment polarity network is a robust developmental module. *Nature* **406**, 188-192 (2000).

12 Grafahrend-Belau, E. *et al.* Multiscale metabolic modeling: dynamic flux balance analysis on a whole-plant scale. *Plant Physiol* **163**, 637-647, doi:10.1104/pp.113.224006 (2013).

13 Band, L. R. *et al.* Systems analysis of auxin transport in the Arabidopsis root apex. *Plant Cell* **26**, 862-875, doi:10.1105/tpc.113.119495 (2014).

14 Green, R. M., Tingay, S., Wang, Z. Y. & Tobin, E. M. Circadian rhythms confer a higher level of fitness to Arabidopsis plants. *Plant Physiol* **129**, 576-584. (2002).

15 Nakamichi, N. *et al.* PSEUDO-RESPONSE REGULATORS 9, 7, and 5 are transcriptional repressors in the Arabidopsis circadian clock. *Plant Cell* **22**, 594-605 (2010).

16 Pokhilko, A. *et al.* The clock gene circuit in Arabidopsis includes a repressilator with additional feedback loops. *Mol Syst Biol* **8**, 574, doi:10.1038/msb.2012.6 (2012).

17 Chew, Y. H. *et al.* An augmented Arabidopsis phenology model reveals seasonal temperature control of flowering time. *New Phytol* **194**, 654-665, doi:10.1111/j.1469-8137.2012.04069.x (2012).

18 Christophe, A. *et al.* A model-based analysis of the dynamics of carbon balance at the whole-plant level in Arabidopsis thaliana. *Functional Plant Biology* **35**, 1147-1162, doi:Doi 10.1071/Fp08099 (2008).

19 Nakamichi, N. *et al.* Arabidopsis clock-associated pseudo-response regulators PRR9, PRR7 and PRR5 coordinately and positively regulate flowering time through the canonical CONSTANS-dependent photoperiodic pathway. *Plant Cell Physiol* **48**, 822-832, doi:10.1093/pcp/pcm056 (2007).

20 Niwa, Y., Yamashino, T. & Mizuno, T. The circadian clock regulates the photoperiodic response of hypocotyl elongation through a coincidence mechanism in Arabidopsis thaliana. *Plant Cell Physiol* **50**, 838-854 (2009).

21 Graf, A., Schlereth, A., Stitt, M. & Smith, A. M. Circadian control of carbohydrate availability for growth in Arabidopsis plants at night. *Proc Natl Acad Sci U S A* **107**, 9458-9463, doi:10.1073/pnas.0914299107 (2010).

22 Sulpice, R. *et al.* Arabidopsis coordinates the diurnal regulation of carbon allocation and growth across a wide range of photoperiods. *Mol Plant* **7**, 137-155, doi:10.1093/mp/sst127 (2014).

23 Scialdone, A. *et al.* Arabidopsis plants perform arithmetic division to prevent starvation at night. *Elife* **2**, e00669, doi:10.7554/eLife.00669 (2013).

24 Zell, M. B. *et al.* Analysis of Arabidopsis with highly reduced levels of malate and fumarate sheds light on the role of these organic acids as storage carbon molecules. *Plant Physiol* **152**, 1251-1262, doi:10.1104/pp.109.151795 (2010).

25 Ishihara, H., Obata, T., Sulpice, R., Fernie, A. R. & Stitt, M. Quantifying Protein Synthesis and Degradation in Arabidopsis by Dynamic (CO2)-C-13 Labeling and Analysis of Enrichment in Individual Amino Acids in Their Free Pools and in Protein (vol 168, pg 74, 2015). *Plant Physiol* **168**, 1179-1179, doi:10.1104/pp.15.00771 (2015).

26 Comparot-Moss, S. *et al.* A putative phosphatase, LSF1, is required for normal starch turnover in Arabidopsis leaves. *Plant Physiol* **152**, 685-697, doi:10.1104/pp.109.148981 (2010).

27 Haydon, M. J., Mielczarek, O., Robertson, F. C., Hubbard, K. E. & Webb, A. A. Photosynthetic entrainment of the Arabidopsis thaliana circadian clock. *Nature* **502**, 689-692, doi:10.1038/nature12603 (2013).

28 Fukushima, A. *et al.* Impact of clock-associated Arabidopsis pseudo-response regulators in metabolic coordination. *P Natl Acad Sci USA* **106**, 7251-7256, doi:10.1073/pnas.0900952106 (2009).

29 Le Novere, N. Quantitative and logic modelling of molecular and gene networks. *Nat Rev Genet* **16**, 146-158, doi:10.1038/nrg3885 (2015).

30 Flis, A. *et al.* Defining the robust behaviour of the plant clock gene circuit with absolute RNA timeseries and open infrastructure. *Open Biol* **5**, doi:10.1098/rsob.150042 (2015).

Additional references from Methods

31 Schneider, C. A., Rasband, W. S. & Eliceiri, K. W. NIH Image to ImageJ: 25 years of image analysis. *Nat. Meth.* **9**, 671-675, doi:Doi 10.1038/Nmeth.2089 (2012).

32 Arrivault, S. *et al.* Use of reverse-phase liquid chromatography, linked to tandem mass spectrometry, to profile the Calvin cycle and other metabolic intermediates in Arabidopsis rosettes at different carbon dioxide concentrations. *Plant J* **59**, 826-839, doi:10.1111/j.1365-313X.2009.03902.x (2009).

33 Pyl, E. T. *et al.* Metabolism and growth in Arabidopsis depend on the daytime temperature but are temperature-compensated against cool nights. *The Plant cell* **24**, 2443-2469, doi:10.1105/tpc.112.097188 (2012).

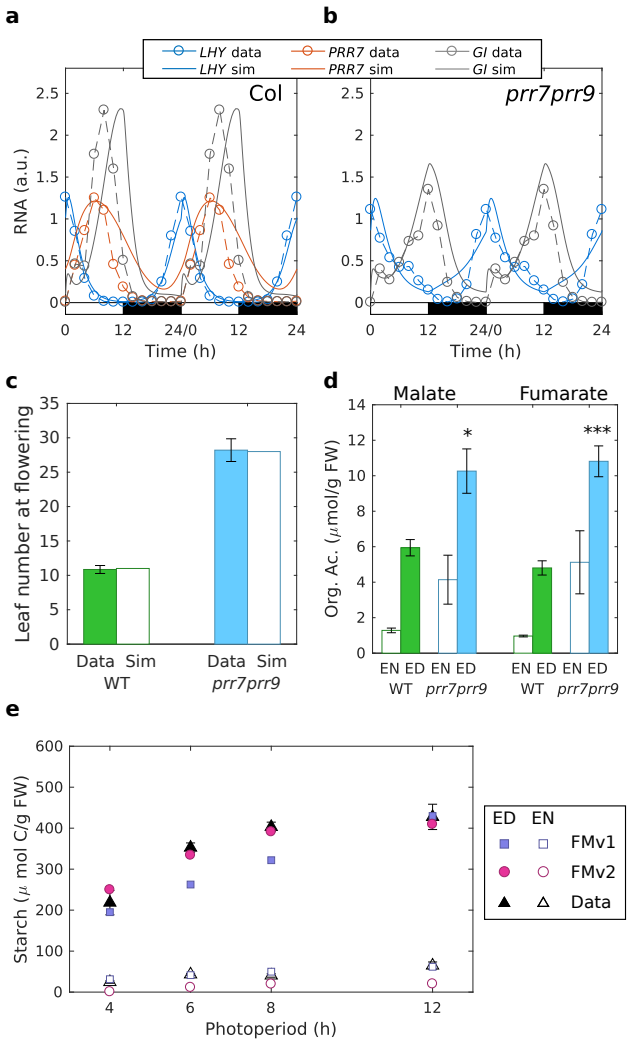

Figure 1: Simulation of clock dynamics and clock outputs.

(a,b) Clock gene mRNA abundance[30] for wild-type (Col) and *prr7prr9* plants (dashed lines, symbols), and FMv2 simulations (solid lines), under 12h light:12h dark cycles (12L:12D), double-plotted, normalised to Col level. (c) Rosette leaf number at flowering[19] under 16L:8D (filled), compared to simulation (open). (d) Malate and fumarate accumulation (mean±SEM, n=4) in Col and *prr7prr9* at end of day (ED) and end of night (EN) under 12L:12D, 20°C, light intensity=160 μmol/m^2/s; t-tests compared *prr7prr9* to Col (* $p<0.05$; *** $p<0.001$). (e) Starch levels at ED (filled) and EN (open) after 30 days under various photoperiods[22] (triangles), compared to FMv1 (squares), FMv2 (circles).

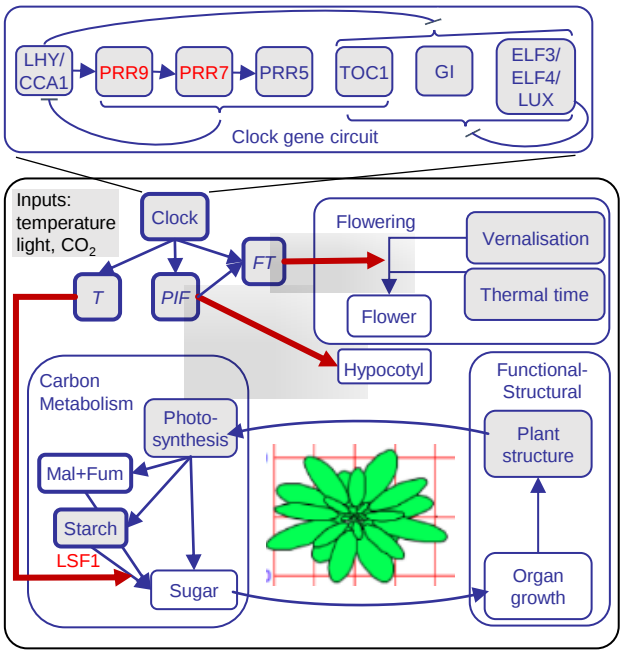

Figure 2: Schematic of the Framework Model.

The FMv2 includes a clock gene circuit sub-model (upper section). Clock outputs (red arrows) regulate hypocotyl elongation via the PIF components, flowering *via FT* mRNA production and starch degradation *via* the timer *T*. Environmental inputs affect multiple model components (shaded). Vegetative growth is driven by the positive feedback on photosynthesis, mediated by sugar-powered growth of photosynthetically active leaf area within the plant structure. The FMv2 includes nightly carbon storage both in starch and in a secondary, organic acid pool, comprising malate and fumarate (Mal+Fum). Components tested by mutation (PRR9, PRR7, LSF1) are shown in red (see Extended Data).

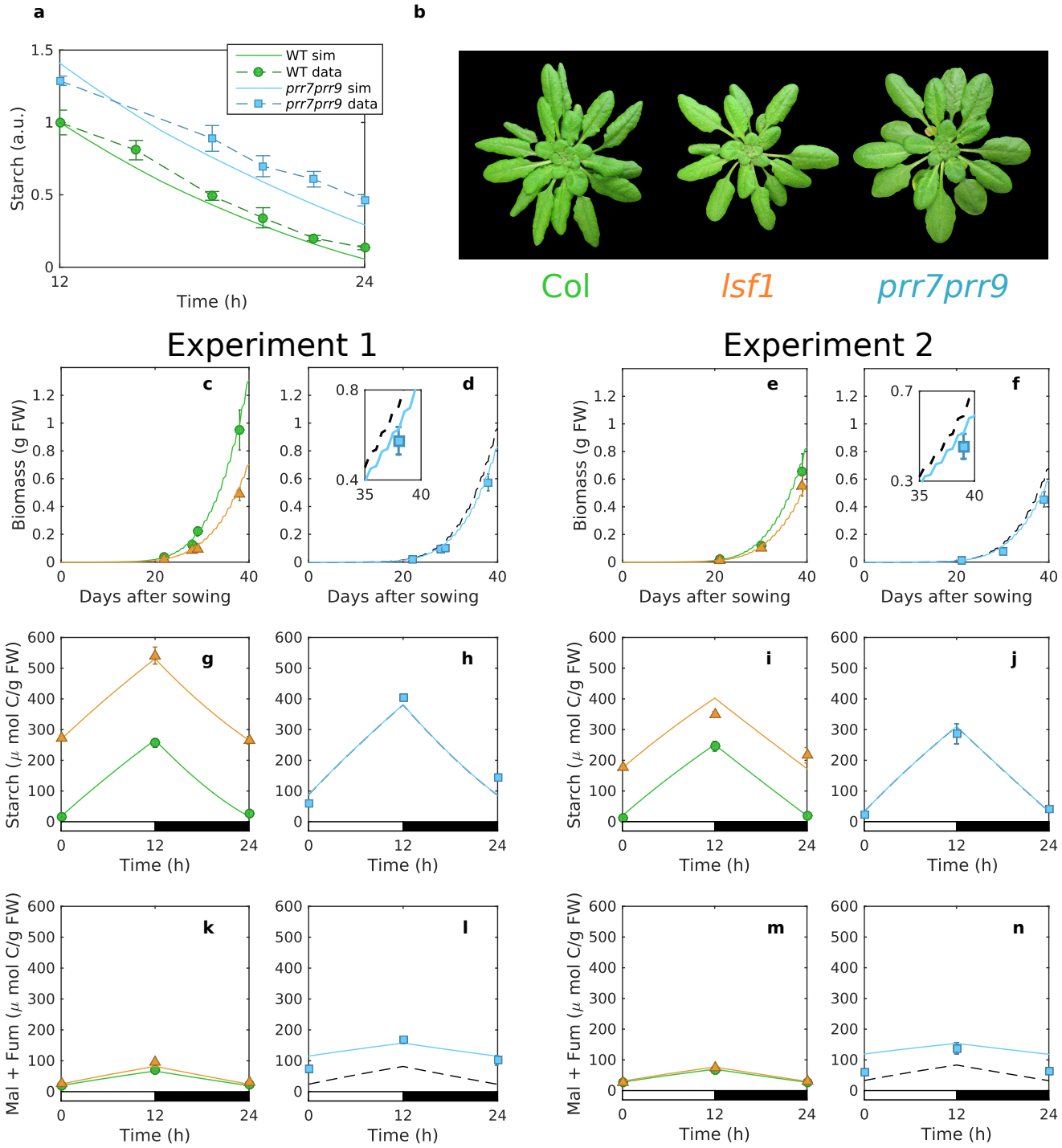

Figure 3: Contributions of starch and organic acids to biomass growth.

(a) *prr7prr9* (blue, squares) mobilised starch more slowly than Col (green, circles); normalised to Col peak (mean±SEM, n=6). (b) 38-day-old Col, *lsf1*, *prr7prr9*. (c-n) Data (symbols) and simulation (lines) of fresh weight (c-f), starch (g-j) and total malate and fumarate (k-n) for Col (circles, green), *lsf1* (triangles, orange) and *prr7prr9* (squares; dashed black, simulation of starch defect; blue, starch and organic acid defects). (d,f) Insets enlarge main panel. Data show mean±SD; n=5 for biomass; n=3 for metabolites, where each sample pooled 3 plants. Temperature=20°C (a), 20.5°C (b, Experiment1), 18.5°C (Experiment2); 12L:12D light intensity=190 μmol/m^2/s (a), 145 μmol/m^2/s (b-n); CO_2=420 ppm.

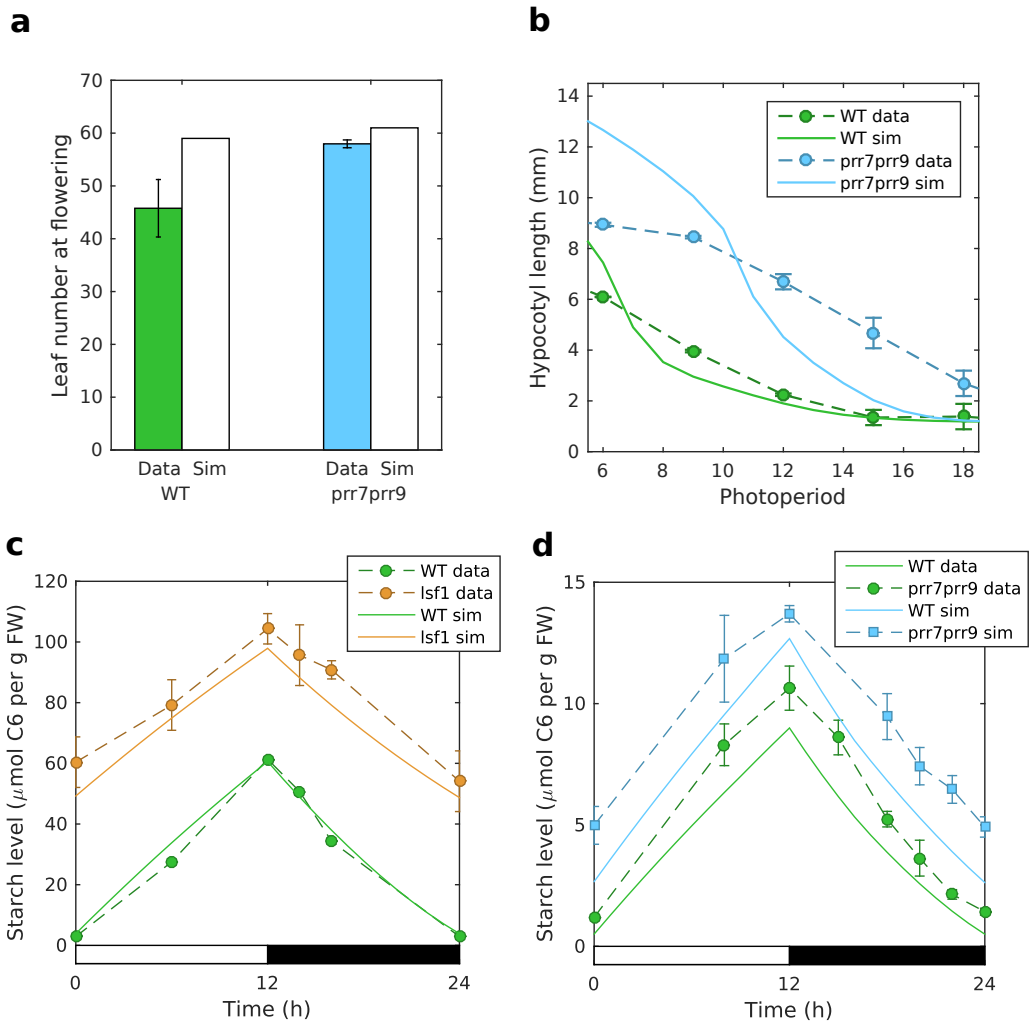

Extended Data Figure 1: Simulation of clock outputs.

(a) Simulated leaf number under short photoperiods for WT and *prr7prr9*, compared to data from (Nakamichi et al, 2007); (b) Simulated hypocotyl elongation in multiple photoperiods, compared to data of (Niwa et al, 2009); (c) starch levels in *lsf1* under 12L:12D, compared to model simulations (Comparot-Moss et al, 2010); (d) Starch levels in *prr7prr9* under 12L:12D, compared to model simulations (as in Fig 1c, plotted in absolute values). Model simulation (lines) and experimental data (symbols) of night-time starch level for Col (green line, filled circles) and *prr7prr9* (blue line, open squares). These are the same data from Fig. 1c. Results are given as mean ± SEM (n = 6). Temperature= 20 °C; light = 190 μmol/m^2/s; photoperiod = 12 hr light: 12 hr dark.

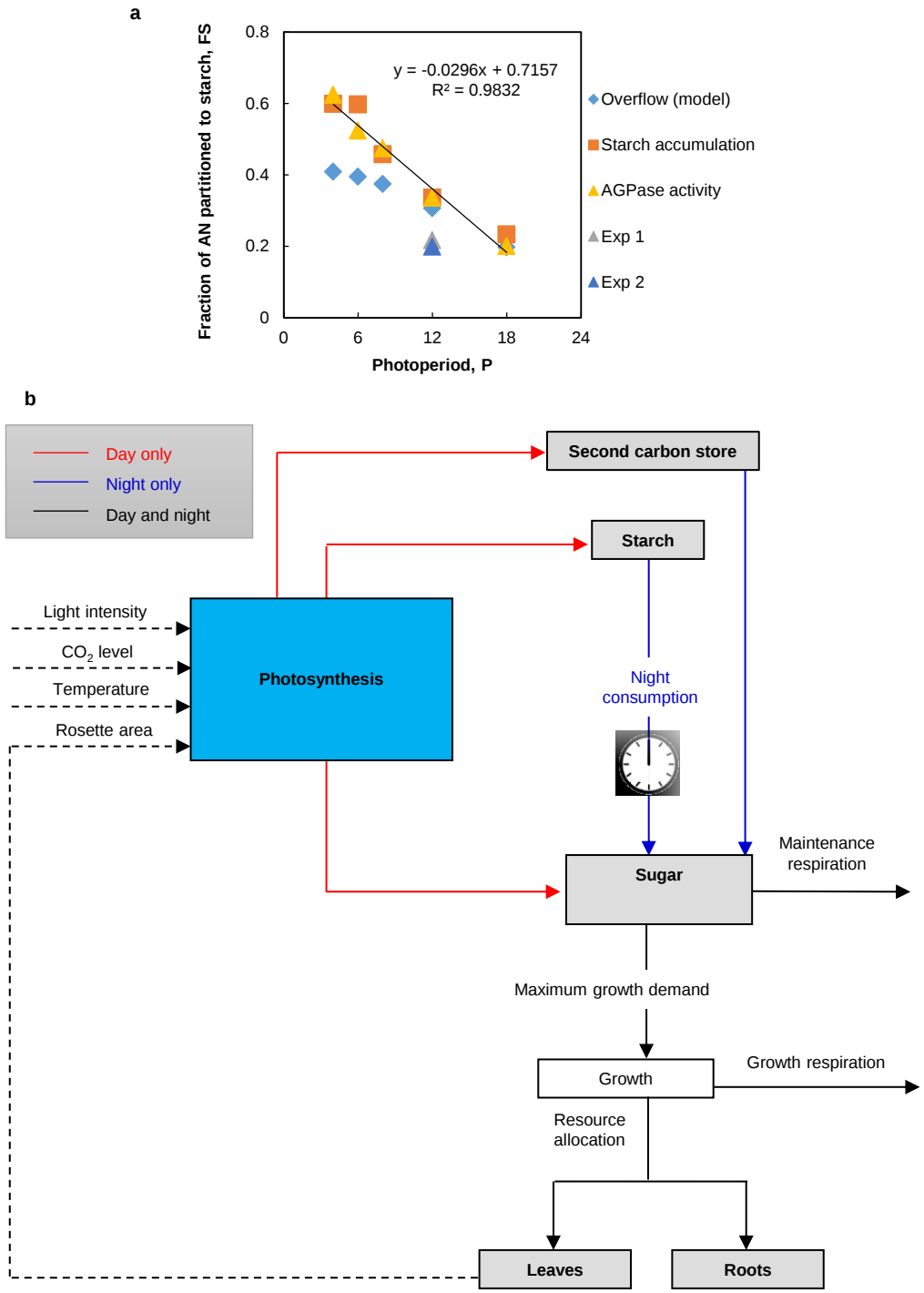

Extended Data Figure 2: Updating the Carbon Dynamic Model (CDM).

(a) The fractions of net assimilate partitioned to starch at different photoperiods, as simulated in the original CDM (FMv1) using the 'overflow' concept, calculated based on measured starch levels and calculated based on measured AGPase activity. The linear regression shown is for the AGPase activity series. The values used subsequently in the model for each experiment (Experiment 1, Experiment 2; Figure 3) are also shown. (b) Schematic of the new Carbon Dynamic Model (CDM). The second carbon store represents the total amount of malate and fumarate. The clock symbol represents the regulation of the rate of starch consumption by the circadian clock model. Dashed arrows indicate information or feedback input.

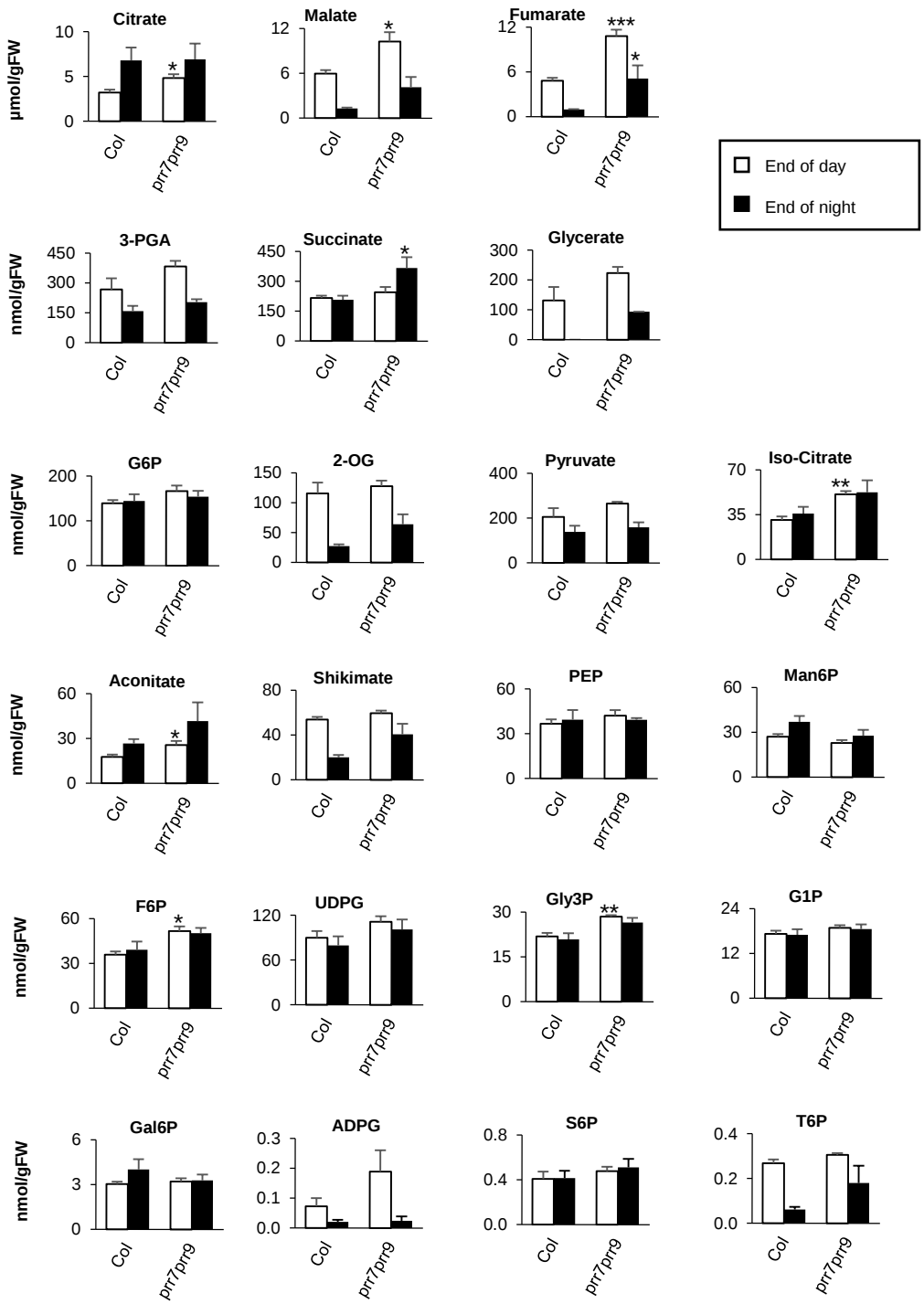

Extended Data Figure 3: Primary metabolites for Col and prr7prr9 mutant measured at the end of day and the end of night.

The results are given as the mean ± SEM (n = 4). Each sample consisted of 5-7 pooled plants. Temperature = 20°C during the day and 18°C during the night; light = 160 μmol/m^2/s; photoperiod = 12 h light: 12 h dark. The *t*-test compared between Col and *prr7prr9* (* $p < 0.05$; ** $p < 0.005$; *** $p < 0.001$). Note that the units given for citrate, malate, and fumarate are μmol/gFW, while the units given for the remaining metabolites are nmol/gFW.

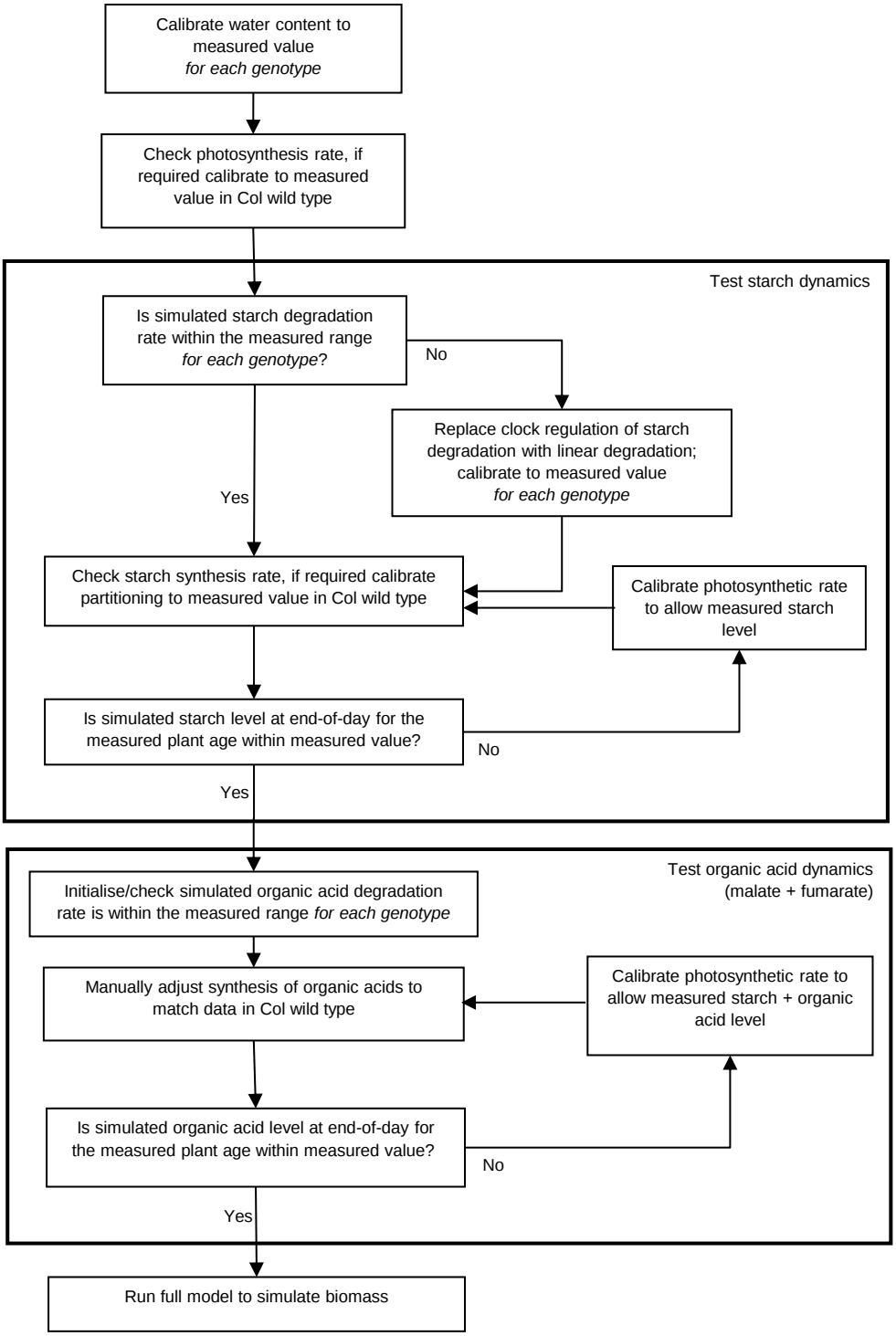

Extended Data Figure 4: Flow diagram of parameter calibration.

Parameters that could be directly or indirectly measured were adjusted in the illustrated sequence, to capture measured carbon dynamics and metabolite levels at specific time points. Once these were achieved, the model was simulated using the determined parameters to generate predictions for plant biomass.

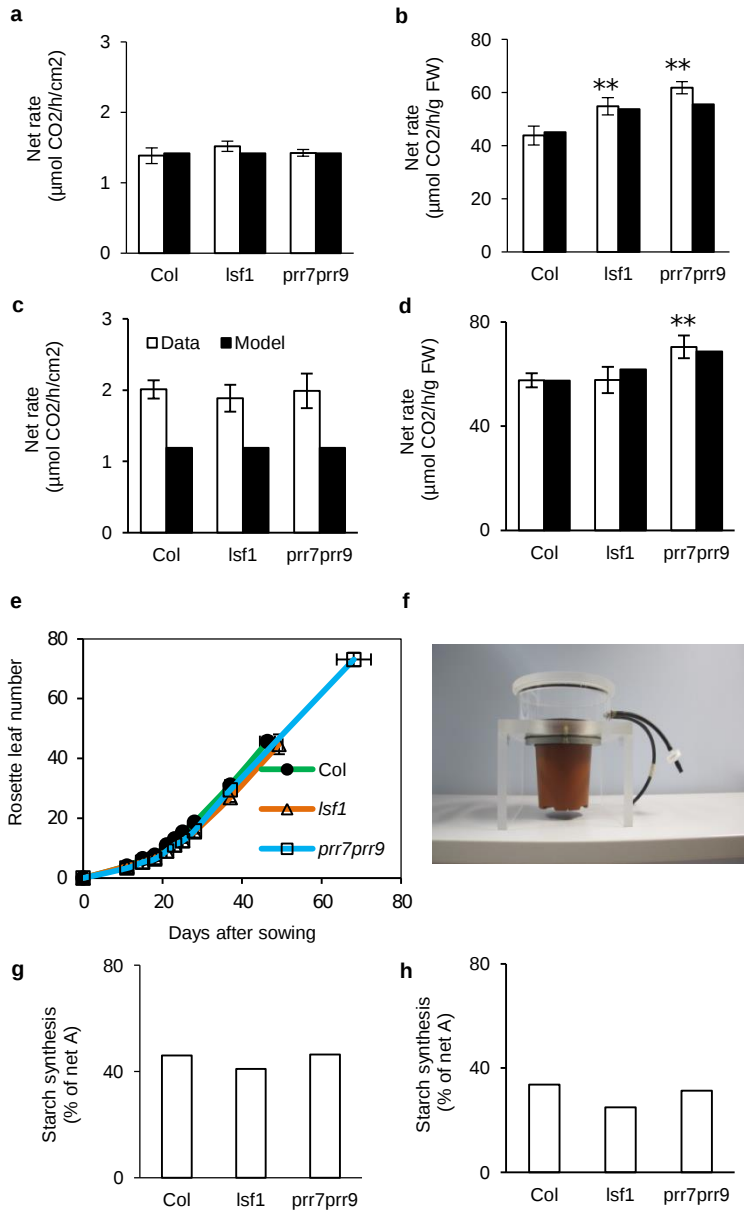

Extended Data Figure 5: Gas exchange measurement and leaf number of different mutants.

Net assimilation rate for Col, *lsf1* and *prr7prr9* in Experiment 1 (a, b) and Experiment 2 (c, d) expressed per unit rosette area (left column) and per gram fresh weight (right column). Data are shown as white bars while model simulations are shown as black bars. Data are given as mean ± SD (n = 5 plants). There were no significant genotypic differences for net assimilation per unit area, thus similar rates were used in model simulations for all genotypes. However, net assimilation per unit fresh weight was significantly higher in *lsf1* and *prr7prr9* (** $p < 0.005$). Taking genotypic differences in water content into account was sufficient for the model to reproduce these results. (e) Rosette leaf number until flowering for Experiment 1. There was no significant difference in the flowering time of *lsf1*, while *prr7prr9* was late-flowering. (f) The Plexiglass chamber used for gas exchange measurement. Starch synthesis as a percentage of net assimilation rate for Experiment 1 (g) and Experiment 2 (h).

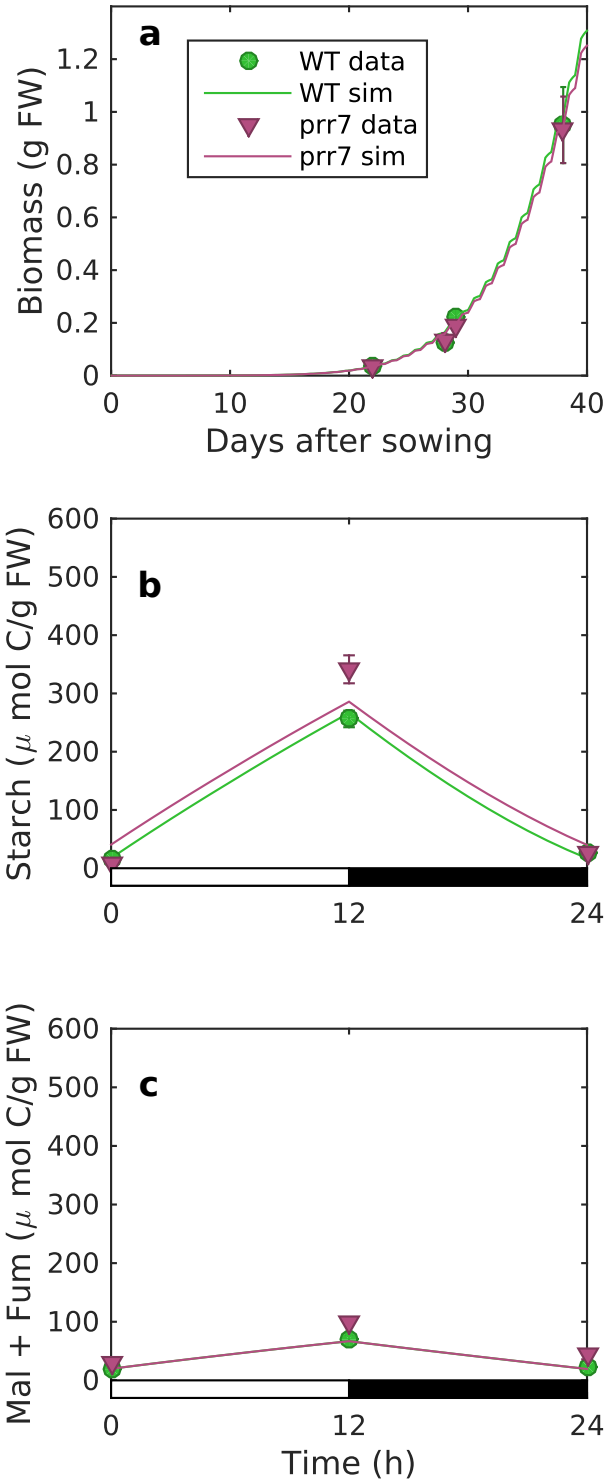

Extended Data Figure 6: Biomass and carbon status of *prr7* mutants.

Measured (symbols) and simulated (lines) fresh weight (a), starch level (b), and malate and fumarate (c) for *prr7* single mutant plants (purple) compared to wild type Col (green) in Experiment 1. Data for Col are identical to Fig.3a,3b.

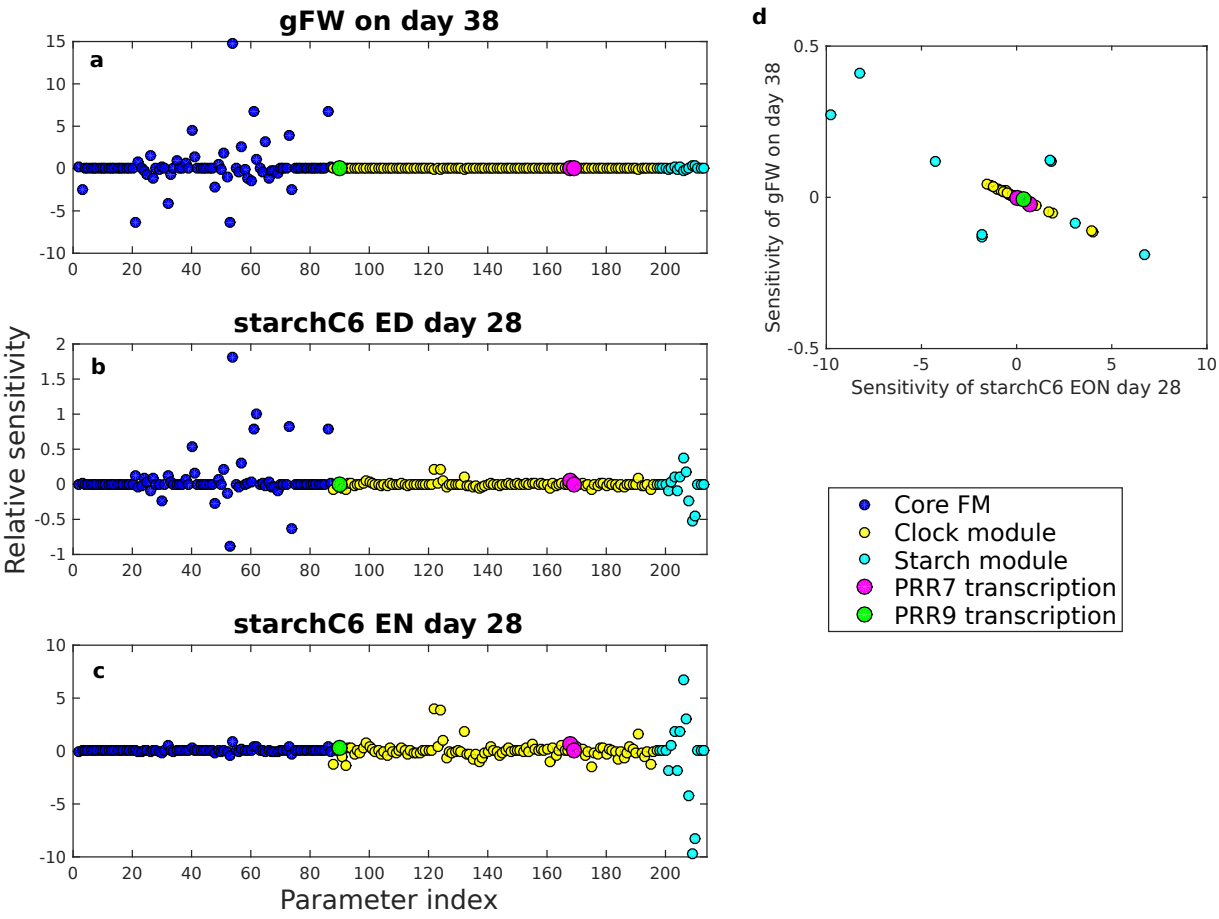

Extended Data Figure 7: Parameter sensitivity overview.

Relative sensitivity of model outputs for each model parameter, coloured by the cognate sub-model (see legend). Sensitivities were calculated by simulating the model under 1% perturbations of each parameter in turn. (a) Fresh Weight (FW); most sensitive parameter is s_{elec}, associated with electron transport, (b) starch level at end of day (ED); most sensitive parameter is s_{elec} and (c) at end of night (EN); most sensitive parameter is k_{dT1}, the degradation rate of a putative inhibitor of starch turnover. Clock parameters mutated to simulate *prr7prr9* double mutants are highlighted (see legend). (d) Comparison of sensitivity of FW and EON starch for parameters clock and starch module parameters, showing a predominant negative correlation: parameters that lower starch at the end of the night tend to increase fresh weight. Note that water content (w, a directly measured parameter) is not shown due to high sensitivity. Sensitivities to changes in water content were 11.3, -10.1, and -10.1 for gFW, ED starch, and EN starch, respectively.

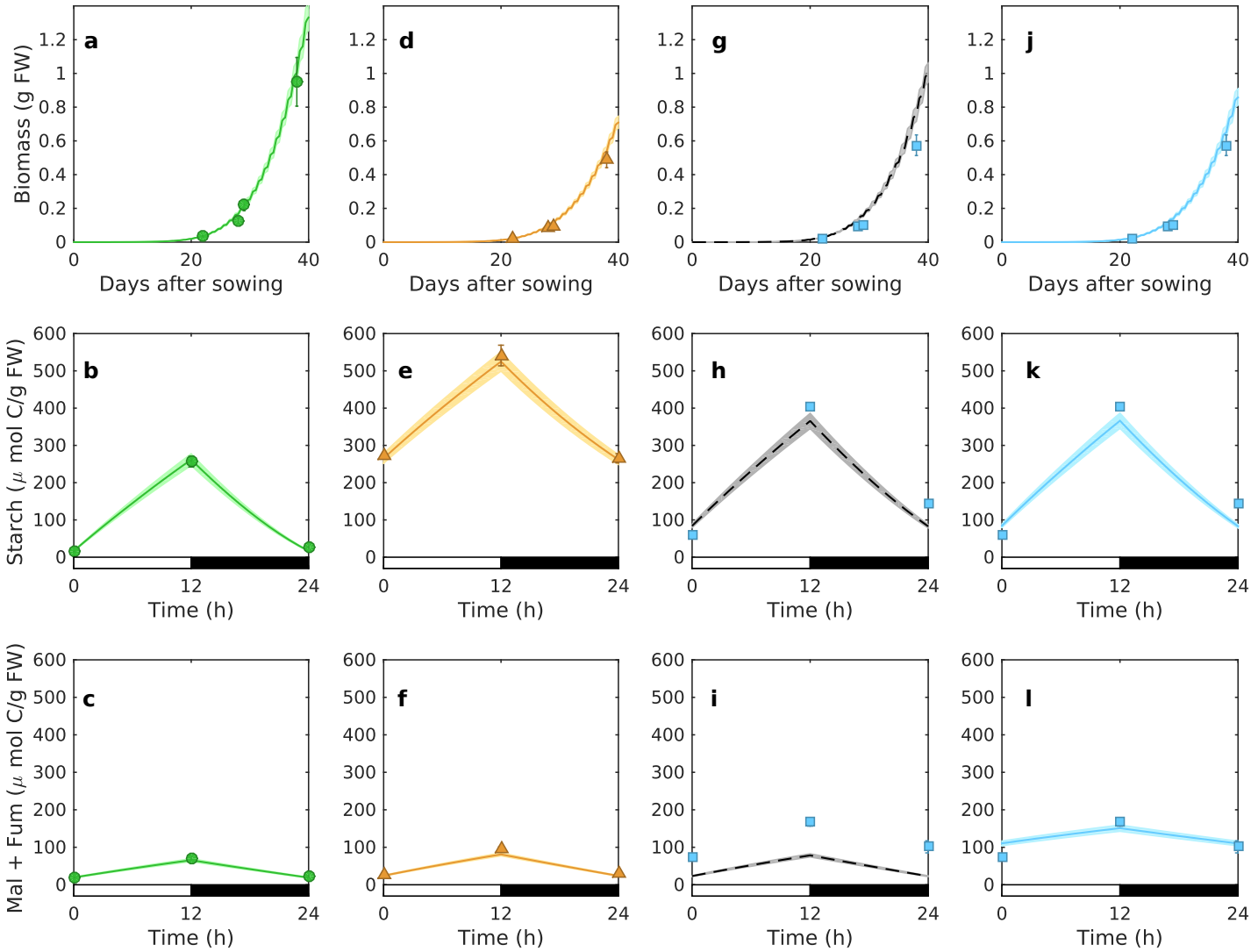

Extended Data Figure 8 : Model sensitivity to water content parameter.

Simulation of biomass and major metabolites using water content values plus and minus one standard deviation from the mean, for Experiment 1 in Figure 3. Model simulation (lines) andexperimental data (symbols) of fresh weight (a,d,g,j), starch level (b,e,h,k) and the total levelof malate and fumarate (c,f,i,l) for Col (a-c), *lsf1* (d-f) and *prr7prr9* (g-l). Dashed lines (g-i) are model simulation for *prr7prr9* that only considered starch defects, while full lines (j-l) are model simulation that included both starch defects and inefficient use of malate and fumarate. Shaded regions indicate the values spanned by simulating water contents plus and minus one standard deviation from the mean. Data are given as mean ± SD (n = 5 for biomass; n = 3 for metabolites with each sample consisting of 3 pooled plants). Temperature = 20.5°C; light=145 μmol/m^2/s; photoperiod = 12 hr light: 12 hr dark; CO_2 = 420 ppm.

Extended Data Table 1 | New parameters and their calibrated values for each experiment, and model goodness-of-fit (cvRMSE)

			Experiment 1		Experiment 2	
Genotypes	Parameters	Parameter names in model file	Calibrated values	Remarks	Calibrated values	Remarks
Col (default)	Photosynthesis efficiency	photosyn_efficiency	0.88	Calculated from Col data	0.79	Calculated from Col data
	Starch synthesis efficiency	ss_efficiency	0.6	To fit the ED Col starch level	0.55	To fit the ED Col starch level
	Starch turnover*	sta_turnover	NA	Simulated with clock-regulated starch model	0.92	Calculated from data
	MF turnover	mf_use	0.7	Calculated from data	0.6	Calculated from data
	MF synthesis	mf_syn_frac	0.2	Calculated from Col data	0.2	Calculated from Col data
	Water content (%)	w	91.16	Measured	89.99	Measured
	cvRMSE (%)		8.0		16.0	
lsf1	Starch turnover*	sta_turnover 0.84 in FMv1; clock-regulated model in FMv2	Clock-regulated model $k_{d,S}$ = 10 $k_{d,T,2}$ = 0.018	To fit the ED and EN starch levels	sta_turnover 0.56	To fit the ED and EN starch levels
	Water content (%)	w	89.43	Measured	89.25	Measured
	cvRMSE (%)		13.7		15.4	
prr7/prr9	Starch turnover*	sta_turnover	NA	Simulated clock mutations control starch *via* clock-regulated starch model	0.89	To fit the ED and EN starch levels
	Water content (%)	w	89.12	Measured	88.04	Measured
	MF turnover	mf_use	0.25	To fit the ED MF level	0.21	To fit the ED MF level
	cvRMSE (%)		41.1	Simulation with only starch defects	44.8	Simulation with only starch defects
	cvRMSE (%)		15.1	Simulation with defects in starch, malate and fumarate consumption	20.9	Simulation with defects in starch, malate and fumarate consumption

*The sta_turnover parameter in FMv1 (value 0.84) is not used in FMv2, because starch degradation rate is computed by the clock-regulated starch model. Where *prr7prr9* showed a mild starch phenotype, in experiment 2, sta_turnover was calibrated as described in Extended Data Fig.4; the same model was used to compare all genotypes in the experiment.

Supplementary methods – modelling

Contents

Supplementary methods – modelling....1
1. Updating the circadian clock, starch, and photoperiod response models....1
1.1 Photoperiod response model....1
1.2 Circadian control of starch turnover....2
2. Revision of Starch synthesis....3
3. Addition of carbon pool for malate and fumarate....4
4. Parameter calibration....4
5. Modelling protein synthesis, compared to literature data....5
6. References....6

1. Updating the circadian clock, starch, and photoperiod response models

1.1 Photoperiod response model

The circadian clock controls the timing of flowering by regulating the expression of the *FT* gene through the photoperiod pathway. The photoperiod response was previously modelled in the Arabidopsis Framework Model version 1 (FMv1) [1] by including the model from Salazar et al 2009 [2]. However, this model includes an older circadian clock model [3] that does not explicitly represent the relevant clock components *PRR9* and *PRR7*. We therefore replaced the Salazar model with our most recent, Seaton-Smith model of the photoperiod pathway [4]. This brings several advantages. First, the Seaton-Smith model includes additional understanding of the photoperiod response mechanism, such as the regulation of CO protein stability by FKF1 [5]. Second, it is based upon the same circadian clock model [6] as the clock-starch model that we introduce in Section 1.2, below. Third, the clock model includes *PRR9* and *PRR7*, allowing explicit simulation of the *prr9prr7* mutation (see section 1.2.2). Fourth, the Seaton-Smith model represents circadian regulation of hypocotyl elongation via the *PIF* transcription factors, allowing the FMv2 to represent this canonical clock phenotype.

As in the Salazar and FMv1 models, the photoperiod response model in the FMv2 interacts with the phenology model through the control of *FT* transcript expression. The important characteristic is '*FTarea*', the integrated *FT* level over the course of a 24h day. *FTarea* controls the *Photoperiod* component of the phenology model through the expression:

$$Photoperiod = a + b\left[\frac{c^n}{c^n + FTarea^n}\right]$$

In order to utilise this connection with the new circadian clock model, the parameters *b, c* and *n* were chosen so that this function matched the original photoperiod function given by Chew et al 2012 [7], as was done previously for the connection from the older clock model in Chew et al 2014 [1].

1.2 Circadian control of starch turnover

The circadian clock controls the rate of starch degradation during the night in light:dark cycles [8,9]. The molecular mechanisms responsible for this control have not been identified, but our recent work identified simple, plausible mechanisms [10]. These were formalised in mathematical models that were evaluated by comparison to a wide range of experimental data (e.g. the change in starch turnover when dusk arrives ~4 hours early). In Seaton et al 2014 [10], three models were described in detail, named Model Variants 1, 2 and 3. Of these, Model Variants 2 and 3 provided the best match to experimental data, while Model Variant 1 was shown to have several limitations. Since Model Variants 2 and 3 provided quantitatively similar predictions over a range of conditions, and Model Variant 2 is simpler (6 fewer parameters and 2 fewer regulatory links from the circadian clock), we chose to integrate Model 2 with the FMv2.

1.2.1 Starch model structure

In order to incorporate this control of starch turnover with the FM, we treat the starch component S as a measure of starch concentration (rather than absolute quantity per plant). Thus, this is taken as:

$$S(t) = r\frac{C_{starch}(t)}{C_{shoot}(t)}$$

Where S(t) is starch concentration variable used in the model of starch turnover, C_{starch}(t) and C_{shoot}(t) are the carbon in starch and in the shoot biomass respectively, and r is a scaling factor used to bring S(t) to a similar range of concentrations to those used in the original model construction[10]. Note, the control of starch synthesis by the species Y is disregarded, as starch synthesis is modelled as a fixed fraction of photoassimilate (see Section 1.2).

This model runs on an hourly basis throughout the day, but controls starch turnover only during the night. The starch concentration (i.e. $S(t)$) is calculated at the start of the timestep, and the change in starch levels by the end of the hour is then given by:

$$\Delta C_{starch}(t) = \frac{C_{shoot}(t)\Delta S(t)}{r}$$

Where $\Delta S(t)$ denotes the change in starch concentration across the hour of simulation. Total starch carbon at the following timepoint is then updated according to:

$$C_{starch}(t+1) = C_{starch}(t) + \Delta C_{starch}(t)$$

1.2.2 Simulating *lsf1* and *prr7prr9* mutant genotypes

In order to simulate the circadian clock mutant *prr7prr9*, we set to 0 the clock parameters q_3, n_4, n_7, n_8, and n_9, which control the multiple aspects of the transcription rate of *PRR7* and *PRR9*. Model simulations predicted ~70% turnover of starch in the mutant, in agreement with experimental data (Fig. 3a and Extended Data Figure 1d).

All other parameter values were calibrated as described in Section 4, below (Extended Data Fig.4), and are shown in Extended Data Table 1. The starch degradation rate parameter in FMv1 (*sta_turnover*) is not used in FMv2, because the starch degradation rate is computed by

the clock-regulated starch model. In order to simulate the *lsf1* mutant, the parameters $k_{d,S}$ and $k_{d,T,2}$ in this model were set to 10 and 0.018, respectively, calibrating simulated starch to our experimental data. This allowed the model to match the experimentally observed starch turnover in our experiment 1 (Fig. 3g) and in literature data [11] (Extended Data Figure 1c). Where *prr7prr9* showed a mild starch phenotype in experiment 2, *sta_turnover* was calibrated as described in Extended Data Fig.4; the same model was used to compare all genotypes in the experiment.

2. Revision of Starch synthesis

In the original Carbon Dynamic Model (CDM) [1,12], starch is synthesised at a rate that is the sum of a baseline rate and an 'overflow' rate. The baseline rate is a fixed proportion of the photoassimilate. The rest of the photoassimilate is first converted into soluble sugars which are used for growth and respiration. As growth demand is limited to a maximum value, any excess photoassimilate is converted into starch, through the 'overflow' rate.

Our previous work [1,13] showed that the 'overflow' mechanism is not always applicable, especially when plants are grown in short-day conditions (Figure 1e). Results suggested that starch is synthesised at a photoperiod-dependent fixed rate that is much higher than the baseline, and any excess photoassimilate remains as sugars. This ensures that plants store sufficient starch to last the night. We therefore re-routed the carbon flow based on this finding.

To determine the photoperiod-dependent starch synthesis rate, we first calculated the fraction of measured net assimilate partitioned to starch using our previous data[13] and the equation below:

$$F_S = \frac{S_{ED} - S_{EN}}{A_N \times P}$$

where

F_S	=	Fraction partitioned to starch
S_{ED}	=	Starch level at ED
S_{EN}	=	Starch level at EN
A_N	=	Net assimilation rate per hour
P	=	Photoperiod

It has been reported that under low light conditions, most of the flux control through the pathway of starch synthesis resides in the reaction catalysed by AGPase [14]. Since most lab experiments are conducted under low light, we therefore also tested the relation between the fraction partitioned to starch and AGPase activity. If the total amount of starch accumulated over the light period is proportional to daily AGPase activity (averaged between ED and EN), the fraction is given by:

$$F_S(P) = \frac{k[AGPase_{average}(P)]}{A_N \times P}$$

where k is the proportional constant. We determined the value of k using data from 12-hr photoperiod as the reference. We found a strong linear relation between the fraction of measured net assimilate and photoperiod (Extended Data Figure 2). This relation is therefore used in the FMv2 to determine starch synthesis rate, *StaSyn*, as follows:

$$StaSyn = A_N \times (-0.0296P + 0.7157)$$

3. Addition of carbon pool for malate and fumarate

Malate and fumarate can be interconverted in the tricarboxylic acid cycle, so they are considered together in a single pool. The dynamics of this pool is modelled in a manner similar to starch except for the regulation of degradation rate by the clock. In the daytime, a fixed proportion of the photoassimilate is converted to starch, malate and fumarate, while sugar level is allow to fluctuate depending on the carbon excess. At night, malate and fumarate are consumed with a linear rate, while starch degradation rate is controlled by the clock sub-model (see Extended Data Figure 2 and Section 1.2). For simplicity, we model a direct conversion of carbon from malate and fumarate into sugar at night, omitting the intermediate metabolic reactions.

4. Parameter calibration

Results in our previous studies [1,13] suggested that carbon dynamics in plants are flexible and plants adjust processes like photosynthesis, starch synthesis and starch degradation rate depending on the environment. The aims of our study were to test if the dynamics of the different carbon pools can be quantitatively balanced over the timescale of vegetative growth, and how genetic regulation that modifies these dynamics affects plant growth. It is therefore necessary that the model first matches quantitatively the carbon pool data for wild-type plants as the reference genotype in each study. After accounting for environmental effects on all genotypes through the wild-type data, discrepancies between model simulations and data for the mutants can be attributed to genetic effects. To achieve this, we calibrated the following to the Col data (workflow illustrated in Extended Data Figure 4; parameter values in Extended Data Table 1):

- photosynthesis rate was adjusted by introducing an efficiency factor relative to the default
- starch synthesis rate was adjusted by introducing an efficiency factor relative to the default

Starch turnover was simulated by the clock-controlled starch submodel (Section 1.2), which reproduced experimental measurement of percentage turnover in most cases. In cases where the phenotype of starch degradation was too mild and could not be explained by the starch submodel, we used a linear degradation rate as in the previous model version (FMv1) to

reproduce the turnover. We then iteratively tuned starch synthesis and photosynthesis rates to match the measured end-of-day level (Extended Data Table 1).

We next calibrated the parameter values for the new carbon pool that represents malate and fumarate (MF) using Col data as follows:

- The initial level of this pool was set as 0.4 of initial starch level, based on the ratio measured in the literature [15]
- MF synthesis was set as a fixed fraction of starch synthesis
- MF turnover was set as the fraction of dusk level consumed

Wherever possible, we used parameter values measured or calculated from our data. Mutants were simulated by changing the values of genotype-specific parameters as listed in Extended Data Table 1, notably the water content.

In each experiment, we did not find genotypic differences in photosynthesis when expressed per unit area, but there was a general increase in photosynthesis in *prr7prr9* when expressed per gram fresh weight (Extended Data Figure 5). Even though we used the same photosynthesis efficiency for all genotypes, we found that the model could reproduce this increase due to the lower water content measured in *prr7prr9*. This suggested the importance of including water content as a genotype-specific parameter in our model, since metabolites are measured per unit fresh weight.

As expected, we found variation in photosynthesis efficiency between experiments. In particular, the photosynthesis per unit area was higher for all genotypes in Experiment 2. As a result, the model underestimated these, but reproduced the values when expressed per unit fresh weight, suggesting a difference in the specific leaf area.

5. Modelling protein synthesis, compared to literature data

The biomass prediction in the FMv2 implies minimal budgets for the nutrient constituents of biomass, which are effectively predictions that can be compared to published experimental data. For example, $^{13}CO_2$ labelling has allowed quantification of the relative rates of protein synthesis in the light and dark during light:dark cycles [16], and of rates of protein turnover [17].

The model does not include protein as a distinct component of the synthesised biomass. However, since the protein fraction of biomass is relatively constant across the course of a day (for example, see Pyl et al 2012 [18]), and protein turnover has been measured, it is possible to calculate an implied rate of protein synthesis for a given model simulation (as done experimentally in Ishihara et al 2015 [17]). In particular:

$$ProtSyn(t) = (Gr(t) + Turn)\ Prot$$

where *ProtSyn*(*t*) is the calculated rate of protein synthesis at time *t*, in units of gProtein gFW^{-1} h^{-1}. *Gr*(*t*) is the relative growth rate (= *(Biomass(t)-Biomass(t-1))/Biomass(t)*), in units of hr^{-1}. *Turn* is the rate of protein turnover, measured as 0.0014 hr^{-1} (average of measurements by Pulse-Chase labelling [17]). *Prot* is the protein content, measured as 0.0169 gProtein gFW^{-1} in Ishihara et al 2015 [17].

Simulating the conditions used in Ishihara et al 2015 [17] for wild-type plants shows that carbon biomass growth rates in the model predict a 3.3-fold increase in the rate of protein synthesis

during the day, compared to during the night. This is in excellent agreement with experimental data which showed a 3.1-fold increase[17], [18].

6. References

1 Chew, Y. H. *et al.* Multiscale digital Arabidopsis predicts individual organ and whole-organism growth. *P Natl Acad Sci USA* **111**, E4127-E4136, doi:10.1073/pnas.1410238111 (2014).

2 Salazar, J. D. *et al.* Prediction of Photoperiodic Regulators from Quantitative Gene Circuit Models. *Cell* **139**, 1170-1179, doi:10.1016/j.cell.2009.11.029 (2009).

3 Locke, J. C. W. *et al.* Extension of a genetic network model by iterative experimentation and mathematical analysis. *Mol Syst Biol* **1**, doi:10.1038/Msb4100018 (2005).

4 Seaton, D. D. *et al.* Linked circadian outputs control elongation growth and flowering in response to photoperiod and temperature. *Mol Syst Biol* **11** (2015).

5 Song, Y. H., Smith, R. W., To, B. J., Millar, A. J. & Imaizumi, T. FKF1 conveys timing information for CONSTANS stabilization in photoperiodic flowering. *Science* **336**, 1045-1049, doi:10.1126/science.1219644(2012).

6 Pokhilko, A. *et al.* The clock gene circuit in Arabidopsis includes a repressilator with additional feedback loops. *Mol Syst Biol* **8**, doi:10.1038/Msb.2012.6 (2012).

7 Chew, Y. H. *et al.* An augmented Arabidopsis phenology model reveals seasonal temperature control of flowering time. *New Phytol* **194**, 654-665, doi:10.1111/j.1469-8137.2012.04069.x (2012).

8 Scialdone, A. *et al.* Arabidopsis plants perform arithmetic division to prevent starvation at night. *Elife* **2**, doi:10.7554/eLife.00669 (2013).

9 Graf, A., Schlereth, A., Stitt, M. & Smith, A. M. Circadian control of carbohydrate availability for growth in Arabidopsis plants at night. *P Natl Acad Sci USA* **107**, 9458-9463, doi:10.1073/pnas.0914299107 (2010).

10 Seaton, D. D., Ebenhoh, O., Millar, A. J. & Pokhilko, A. Regulatory principles and experimental approaches to the circadian control of starch turnover. *J R Soc Interface* **11**, doi:10.1098/Rsif.2013.0979 (2014).

11 Comparot-Moss, S. *et al.* A Putative Phosphatase, LSF1, Is Required for Normal Starch Turnover in Arabidopsis Leaves. *Plant Physiol* **152**, 685-697, doi:10.1104/pp.109.148981 (2010).

12 Rasse, D. P. & Tocquin, P. Leaf carbohydrate controls over Arabidopsis growth and response to elevated CO2: an experimentally based model. *New Phytol* **172**, 500-513, doi:10.1111/j.1469-8137.2006.01848.x (2006).

13 Sulpice, R. *et al.* Arabidopsis Coordinates the Diurnal Regulation of Carbon Allocation and Growth across a Wide Range of Photoperiods. *Mol Plant* **7**, 137-155, doi:10.1093/mp/sst127 (2014).

14 Neuhaus, H. E. & Stitt, M. Control Analysis of Photosynthate Partitioning - Impact of Reduced Activity of Adp-Glucose Pyrophosphorylase or Plastid Phosphoglucomutase on the Fluxes to Starch and Sucrose in Arabidopsis-Thaliana (L) Heynh. *Planta* **182**, 445-454 (1990).

15 Chia, D. W., Yoder, T. J., Reiter, W. D. & Gibson, S. I. Fumaric acid: an overlooked form of fixed carbon in Arabidopsis and other plant species. *Planta* **211**, 743-751 (2000).

16 Pal, S. K. *et al.* Diurnal Changes of Polysome Loading Track Sucrose Content in the Rosette of Wild-Type Arabidopsis and the Starchless pgm Mutant. *Plant Physiol* **162**, 1246-1265, doi:10.1104/pp.112.212258 (2013).

17 Ishihara, H., Obata, T., Sulpice, R., Fernie, A. R. & Stitt, M. Quantifying Protein Synthesis and Degradation in Arabidopsis by Dynamic (CO2)-C-13 Labeling and Analysis of Enrichment in Individual Amino Acids in Their Free Pools and in Protein (vol 168, pg 74, 2015). *Plant Physiol* **168**, 1179-1179, doi:10.1104/pp.15.00771 (2015).

18 Pyl, E. T. *et al.* Metabolism and Growth in Arabidopsis Depend on the Daytime Temperature but Are Temperature-Compensated against Cool Nights. *Plant Cell* **24**, 2443-2469, doi:10.1105/tpc.112.097188 (2012).